Impact of Mistuned Underplatform Dampers on the Nonlinear Vibration of Bladed Disks

Samuel Quaegebeur, Benjamin Chouvion, Fabrice Thouverez

IMPACT OF MISTUNED UNDERPLATFORM DAMPERS ON THE NONLINEAR VIBRATION OF BLADED DISKS

Samuel Quaegebeur,[1,2,*], Benjamin Chouvion[3], and Fabrice Thouverez[1]

[1]École Centrale de Lyon, Laboratoire de Tribologie et Dynamique des Systèmes, UMR CNRS 5513, 36 avenue Guy de Collongue, Écully, 69134, France
[2]Safran Helicopters Engines 64511 Bordes France
[3]Centre de recherche de l'Ecole de l'air, 13300 Salon-de-Provence France

ABSTRACT

Before the final experimental validation and certification of a turboengine, designers perform a numerical simulation of its vibratory properties, among other things, in order to estimate its lifespan and adjust the design in an optimization process. One possible practical solution to decrease the vibratory response is to add underplatform dampers to the system. These components dissipate energy by friction and are widely employed in turbomachinery. However, a specific underplatform damper is usually efficient only for a specific mode. The purpose of this work is to investigate the possibility of adding different kinds of underplatform dampers to the cyclic structure in order to decrease the vibratory energy over a larger panel of modes. Different methods exist to determine the vibrations of nonlinear cyclic symmetric systems, but creating a robust methodology to account for the additional effect of mistuning remains a big challenge in the community. In this paper, the structure is mistuned through the friction coefficient of the dampers and not by altering its geometry, as is usually done in the literature. First, assuming a cyclic symmetric structure, the performance of the dampers is assessed for specific modes. Then, employing a method recently developed, the efficiency of an intentional mistuning pattern of underplatform dampers is studied and an optimal pattern proposed.

Keywords: Underplatform dampers, Mistuning, Reduced-order models, Harmonic Balance

NOMENCLATURE

$\tilde{\mathbf{M}}$, $\tilde{\mathbf{C}}$, $\tilde{\mathbf{K}}$	Mass, damping and stiffness cyclic matrices
$\mathbf{u}$	Nodal displacements vector
$\tilde{\mathbf{u}}$	Spectral displacements vector
$\mathbf{f}_{\text{nl}}$	Nonlinear forces vectors
$\mathbf{x}_{\text{r}}$	Relative contact displacement vector
N	Subscript for the normal direction
T	Subscript for the tangential directions
T	Superscript for the transpose operation
μ	Friction coefficient
$\mathbf{f}_{\text{ext}}$	Vector of external forces
$\mathbf{c}$	Vector of harmonic coefficients for the physical displacement
ω	Excitation frequency
n	Harmonic number index
k	Nodal diameter number index
j	Sector number index
N_{h}	Number of harmonics
h_{ex}	Excitation wave number
N	Number of sectors
μ^*_{1F}, μ^*_{1T}	Optimal value of μ for the 1F and 1T modes
FEM	Finite element model
DOF	Degree of freedom
HBM	Harmonic balance method
SNCR	Substructuring method based on Nonlinear Cyclic Reduction
CNNM	Cyclic normal nonlinear mode
ROM	Reduced-order model
AFT	Alternating frequency time
UPD	Underplatform dampers
CB-CMS	Craig-Bampton Component Mode Synthesis
1F, 1T	First flexural flapwise and torsional modes
DLFT	Dynamic Lagrangian Frequency Time

*Corresponding author: samuel.quaegebeur@ec-lyon.fr

1. INTRODUCTION

Underplatform dampers (UPDs) are key elements in bladed disks as they make the vibratory responses decrease and hence extend the lifespan of the systems. Over the years, the physical mechanisms of UDPs have been investigated [1, 2] and described by different modeling approaches [3–6]. Many parametric studies have also been performed, such as [7, 8] for instance, to examine the influence of the normal load or friction coefficient, or to study the geometrical design of UPDs [3, 9].

In this paper, we focus on the global impact of dampers on the maximal displacement of a cyclic finite-element model (FEM) under harmonic forcing. Simulating the dynamics of the full structure can be very long in the presence of nonlinearities, due to the nonlinear solver which, among other things, must evaluate

the nonlinear forces for all sectors. For perfect cyclic symmetric structures [10, 11], the problem can be transformed from its physical into its spectral quantities. This change of variables significantly reduces the number of unknowns for linear [12] and nonlinear problems [13, 14].

In the case of mistuning [15] – that usually consists of geometrical or material modifications among the sectors, using the cyclic symmetric change of variables may no longer be efficient. Reduced-Order Models (ROMs) have been employed to decrease the size of the FEM while trying to retain sufficient information for accurate results. In linear problems, methods such as the CMM [16] or the IMM [17] are widely used for small random mistuning, whereas the PRIME [18] or more recently the PRISM [19] methods are employed for large mistuning. Unfortunately, these methodologies do not hold for nonlinear problems. Developing ROMs which enable simulation of the dynamics of nonlinear mistuned structures is a challenging task. Different strategies have been proposed [20–23] to tackle this problem. Recently, the authors have developed a new approach called the Substructuring method based on Nonlinear Cyclic Reduction (SNCR) [24] which employs a substructuring approach with cyclic complex nonlinear normal modes.

This paper will use several theoretical and numerical strategies [13, 14, 24] with the following original objective: optimizing an intentional mistuning pattern of UPDs to minimize the maximal displacement of the structure over two distinct modes. The two modes considered are the first flexural flapwise mode (1F) and the first torsional mode (1T). In the literature, such as for instance in [9, 25], damper mistuning is defined by considering different damper geometries. In this paper, the different types of UPDs are distinguished by their friction coefficient. The resolution of this problem is broken down into different subproblems which follow the basic outline of this paper. The methodology is demonstrated on a simplified, yet realistic, finite-element model which is described in Section 2. Section 3 provides the optimal values of the friction coefficient for the two respective modes (1F and 1T modes) seen separately and assuming a perfectly tuned structure. In Section 4, we employ the SNCR to determine an optimal intentional mistuning pattern of the structure. The strategy is presented here on a specific structure but is expected to hold for a large panel of bladed disks. The authors therefore believe it will help turboengineers in the design process.

2. PRESENTATION OF THE TEST CASE

In this paper, we propose to study a bladed disk with underplatform dampers, the fundamental sector of which is represented in Figure 1. The complete system is composed of $N = 24$ sectors.

The model contains 30840 degrees of freedom (DOFs), 712 of which are nonlinear and located on the contact area between the blades and the UPDs. The full bladed disk undergoes a rotational velocity of $2200\,\mathrm{rad\,s^{-1}}$. A Craig-Bampton Component Mode Synthesis (CB-CMS) [26] is applied to reduce the size of the FEM: the nonlinear DOFs, an observation node (taken at the tip of the blade) and the cyclic boundary DOFs (for both the disk and the UPDs) are kept as master DOFs. A modal damping of 5×10^{-4} is applied to the structure for the modes under study.

Figure 2 denotes the natural frequencies of the fully stuck

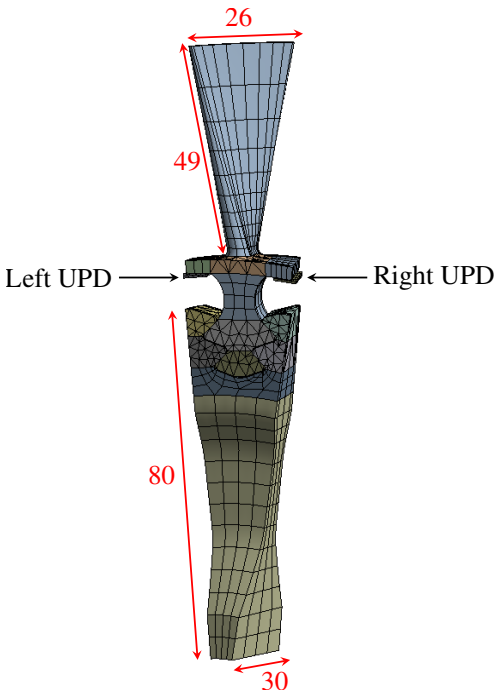

(a) Fundamental sector of the structure.

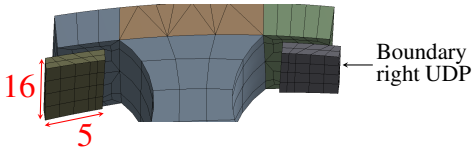

(b) Close-up of the underplatform dampers.

FIGURE 1: DESCRIPTION OF THE MODEL. THE DIMENSIONS ARE IN mm. A PRETWIST ANGLE OF 30° IS APPLIED ON THE BLADE. THE BLADE IS MADE OF ICONEL®738 AND THE DISK OF ICONEL®718.

system (UPDs stuck with the blades, and blade stuck with the disk). Only five families of modes are represented: the first flapwise flexural mode (1F, the blades mainly undergo a transversal motion), the first edgewise flexural mode (1E, both the disk and blade are deformed along the axial direction), the first torsional mode (1T), and the second and third flapwise flexural modes (2F and 3F). In the following, only the 1F and 1T modes of the tenth nodal diameter are studied (as highlighted in red circles in Figure 2).

The excitation on a sector j, noted $\mathbf{f}_{\mathrm{ext},j}$, is composed of a static part $\mathbf{f}_{\mathrm{ext},0}$ (equal for all sectors $j \in [\![1, N]\!]$) representing the centrifugal effects and a harmonic part, noted $\mathbf{f}_{\mathrm{ext,dyn},j}(t)$. The harmonic excitation force can be seen as a simplified aerodynamic force and is applied on a node at the tip of the blades. It follows a traveling wave pattern with a wavenumber $h_{ex} = 10$. The excitation is evaluated with:

$$\mathbf{f}_{\mathrm{ext},1}(t) = \mathbf{f}_{\mathrm{ext},0} + \mathbf{f}_{\mathrm{ext,dyn},1}(t) \tag{1a}$$

$$\mathbf{f}_{\mathrm{ext},j}(t) = \mathbf{f}_{\mathrm{ext},j}\left(t - \frac{2\pi h_{ex}(j-1)}{\omega N}\right) \qquad j \in [\![1, N]\!]. \tag{1b}$$

The excitation on the entire structure is noted $\mathbf{f}_{\mathrm{ext}} =$

$\begin{bmatrix}\mathbf{f}_{\text{ext},1}^T & \cdots & \mathbf{f}_{\text{ext},N}^T\end{bmatrix}^T$ (the superscript T denotes the transpose) and ω is the excitation frequency. To study the 1F mode (respectively 1T), the excitation frequency range will be focused around $2\pi \times 1597\text{rad}\,\text{s}^{-1}$ (respectively $2\pi \times 4860\text{rad}\,\text{s}^{-1}$) and the amplitude of the force is taken as 0.5 N (respectively 1.5 N). The amplitudes were chosen such that the maximal displacements of the linear system (stuck system) are equal for both modes.

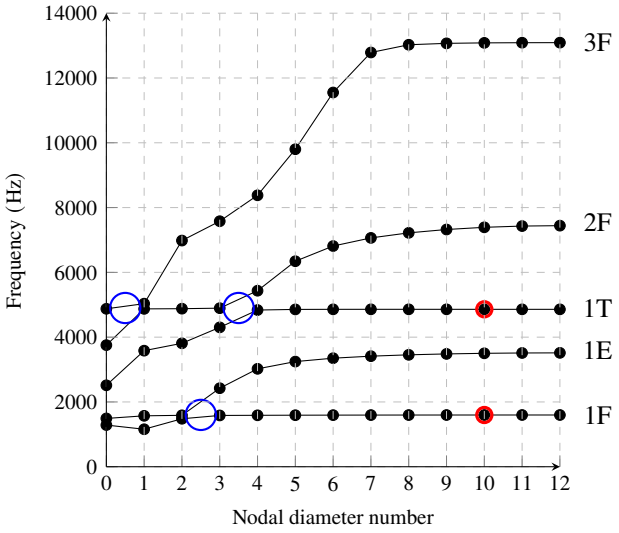

FIGURE 2: NATURAL FREQUENCIES OF EACH NODAL DIAMETER. THE LARGE BLUE CIRCLES DENOTE VEERING AREAS AND SMALL RED CIRCLES DENOTE THE MODES OF INTEREST.

In this work, we focus on the contact between blades and UPDs. The blade/disk contact is therefore simplified and assumed to be always stuck. The UPDs may, however, be either stuck with the blade (the system is then linear and called a stuck system) or account for the following contact/separation law

$$\begin{cases}\mathbf{f}_{\text{nl,N}}(t) \geq 0 & \text{repulsive force only}\\ \mathbf{x}_{r,\text{N}}(t) \geq 0 & \text{no penetration}\\ \mathbf{x}_{r,\text{N}}(t) \cdot \mathbf{f}_{\text{nl,N}}(t) = 0 & \text{either no force or no contact}\end{cases}, \quad (2)$$

where $\mathbf{f}_{\text{nl}}$ defines the nonlinear forces between blades and UPDs, the subscript N denotes the normal direction of the contact, and $\mathbf{x}_r$ represents the relative displacement between both solids on the contact area. If the bodies are in contact, then frictional effects are modeled with the following Coulomb's law,

$$\begin{cases}\|\mathbf{f}_{\text{nl,T}}\| < \mu\left|\mathbf{f}_{\text{nl,N}}\right| & \text{if} \quad \dot{\mathbf{x}}_{r,\text{T}} = 0\\ \mathbf{f}_{\text{nl,T}} = -\mu\left|\mathbf{f}_{\text{nl,N}}\right| \dfrac{\dot{\mathbf{x}}_{r,\text{T}}}{\|\dot{\mathbf{x}}_{r,\text{T}}\|} & \text{if} \quad \|\dot{\mathbf{x}}_{r,\text{T}}\| > 0,\end{cases} \quad (3)$$

where the subscript T denotes the tangential directions and μ is the friction coefficient of the contact interface.

3. PARAMETRIC STUDY ON THE FRICTION COEFFICIENT FOR THE TUNED STRUCTURE

In [27], Krack et al. proposed a novel mathematical approach to optimize dampers based on nonlinear modes for a tuned structure. Although excellent results were demonstrated in [27], several frequency forced responses will be performed here to optimize the friction coefficient. This optimum is defined as the value which minimizes the maximal displacement of the tuned structure. The study is applied for both the 1F and 1T modes. These are first studied separately and hence two optima are obtained. Although this paper proposes to handle mistuning by modifying the friction coefficient, traditional mistuning can naturally be considered (such as modifying the geometry of the dampers and hence the mass, for instance).

3.1 Methodology

In this Section, the structure is perfectly tuned and the cyclic symmetry properties [10, 11] are applied to obtain the different structural cyclic matrices. As underlined in Section 2, the excitation is composed of static and dynamic parts with a wave number equal to 10. This leads to a static load on the zeroth nodal diameter $\tilde{\mathbf{f}}_{\text{ext},0}$, and a dynamic load on the tenth nodal diameter, noted $\tilde{\mathbf{f}}_{\text{ext,dyn},10}$. As demonstrated in [14], the friction nonlinear forces create coupling between different nodal diameters. For the current excitation, the tenth nodal diameter interacts with the second and sixth nodal diameters [14]. The system of equations to be solved then becomes

$$\begin{cases}\tilde{\mathbf{M}}_0\ddot{\tilde{\mathbf{u}}}_0 + \tilde{\mathbf{C}}_0\dot{\tilde{\mathbf{u}}}_0 + \tilde{\mathbf{K}}_0\tilde{\mathbf{u}}_0 + \tilde{\mathbf{f}}_{\text{nl},0} = \tilde{\mathbf{f}}_{\text{ext},0} & \text{(4a)}\\ \tilde{\mathbf{M}}_{10}\ddot{\tilde{\mathbf{u}}}_{10} + \tilde{\mathbf{C}}_{10}\dot{\tilde{\mathbf{u}}}_{10} + \tilde{\mathbf{K}}_{10}\tilde{\mathbf{u}}_{10} + \tilde{\mathbf{f}}_{\text{nl},10} = \tilde{\mathbf{f}}_{\text{ext,dyn},10} & \text{(4b)}\\ \tilde{\mathbf{M}}_k\ddot{\tilde{\mathbf{u}}}_k + \tilde{\mathbf{C}}_k\dot{\tilde{\mathbf{u}}}_k + \tilde{\mathbf{K}}_k\tilde{\mathbf{u}}_k + \tilde{\mathbf{f}}_{\text{nl},k} = \mathbf{0}, \quad k \in \{2,6\}, & \text{(4c)}\end{cases}$$

where $\tilde{\mathbf{M}}_k$, $\tilde{\mathbf{C}}_k$ and $\tilde{\mathbf{K}}_k$ are the mass, damping and stiffness cyclic matrices of the $k-$th nodal diameter. The vectors $\tilde{\mathbf{u}}_k$ and $\tilde{\mathbf{f}}_{\text{nl},k}$ are respectively the $k-$th spectral components of the displacements and nonlinear forces. As the excitation is periodic, we employ the Harmonic Balance Method (HBM) [28] to solve (4) and compute the frequency forced response of the system. The solution on the first sector is sought after as

$$\mathbf{u}_1 = \mathbf{c}_0 + \frac{1}{2}\left(\sum_{n=1}^{N_h}\mathbf{c}_n e^{i\omega t} + \bar{\mathbf{c}}_n e^{-i\omega t}\right), \quad (5)$$

where N_h is the total number of harmonics (here taken equal to 3), and $(\mathbf{c}_n)_{n\in[\![0,N_h]\!]}$ are the harmonic coefficients. The notation $\bar{a}$ denotes the complex conjugate of a. As the excitation follows a traveling wave shape (see Equation (1b)), we assume that the solution also follows the same shape [13]. This allows harmonics numbers and nodal diameters to be paired and thus efficiently reduces the number of unknowns. Applying the HBM and the previous assumption to the system (4) gives:

$$\begin{cases}\tilde{\mathbf{K}}_0\mathbf{c}_0 + \mathbf{c}_{\text{fnl},0} = \mathbf{c}_{\text{fext},0} & \text{(6a)}\\ \left(-\omega^2\tilde{\mathbf{M}}_{10} + i\omega\tilde{\mathbf{C}}_{10} + \tilde{\mathbf{K}}_{10}\right)\mathbf{c}_1 + \mathbf{c}_{\text{fnl},1} = \mathbf{c}_{\text{fext},1} & \text{(6b)}\\ \left(-\omega^2\tilde{\mathbf{M}}_6 + i\omega\tilde{\mathbf{C}}_6 + \tilde{\mathbf{K}}_6\right)\mathbf{c}_3 + \mathbf{c}_{\text{fnl},3} = \mathbf{0} & \text{(6c)}\end{cases}$$

The vectors $\mathbf{c}_{\text{fnl},n}$ and $\mathbf{c}_{\text{fext},n}$ represent the projection of the nonlinear forces and external forces on the harmonic n. The second harmonic is paired with the fourth nodal diameter. However, as

this fourth diameter does not interact with the tenth nodal diameter [14], the associated equation is not retained in the system to be solved. In addition, the tenth nodal diameter interacts with the second nodal diameter, this second nodal diameter is first paired with the fifth harmonic which is beyond the current harmonic expansion ($N_h = 3$).

In this paper, the Dynamic Lagrangian Frequency Time [29] is used as contact algorithm. This procedure assumes no regularization of the friction law (see Equation (3)) and also handles the existence of possible separation (see Equation (2)) between the two bodies in the contact region. This algorithm uses the Schur condensation [30], as well as the Alternating Frequency Time procedure [31].

3.2 Numerical results

The system (6) was solved for different values of μ with excitation frequencies around the 1F and 1T modes which were studied separately. The initial value of μ was taken as equal to 0.3 and was decreased until the optimal value was reached. The optimal values for the 1F and 1T modes, noted μ^*_{1F} and μ^*_{1T}, correspond to the value of μ which minimizes the maximal displacement of the structure for each mode studied separately. Their values were obtained with a precision of 0.01. Figures 3 and 4 represent the maximum response of the structure for a few different values of μ that were simulated.

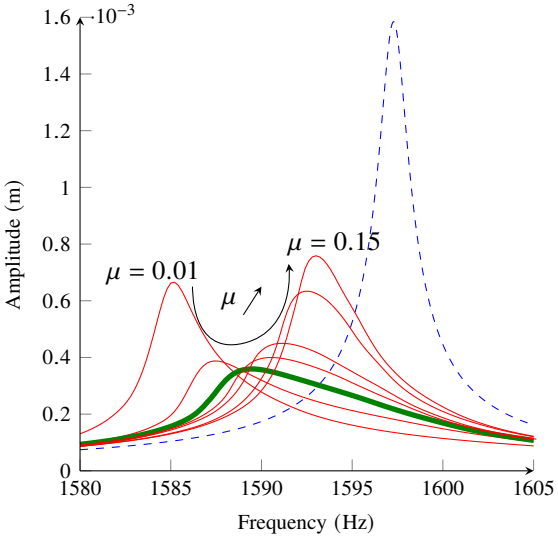

FIGURE 3: FREQUENCY FORCED RESPONSES FOR THE 1F MODE. (- -): LINEAR (STUCK) CASE; ( ): OPTIMAL CASE μ^*_{1F} = 0.03. (—): OTHER VALUES OF μ (0.01, 0.02, 0.04, 0.05, 0.1, AND 0.15 IN THIS ORDER).

The influence of μ on the maximal displacement of the structure has been studied in several papers, see for instance [3]. For high values of μ, the system tends towards the fully stuck structure whereas for very low values, the contact area becomes totally slippery. Between these two limits, an optimal value of μ which minimizes the displacement is reached. For the 1F mode, the optimal value for $\mu^*_{1F} = 0.03$ and for the 1T, $\mu^*_{1T} = 0.1$.

From this preliminary study, two kinds of sector are defined: sector A with a friction coefficient equal to μ^*_{1F} and sector B with a

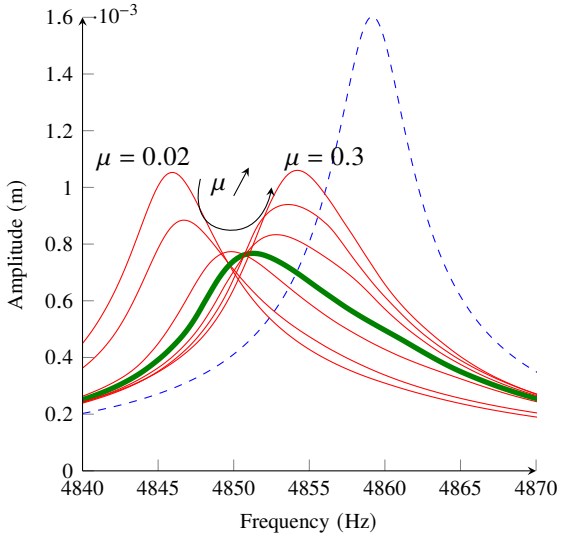

FIGURE 4: FREQUENCY FORCED RESPONSES FOR THE 1T MODE. (- -): LINEAR (STUCK) CASE; ( ): OPTIMAL CASE μ^*_{1T} = 0.1. (—): OTHERS VALUES OF μ (0.02, 0.03, 0.07, 0.15, 0.2, AND 0.3 IN THIS ORDER).

coefficient of μ^*_{1T}. In practise, these different kinds of sectors can be obtained by adding rough and soft patches under the platforms of the blades. The purpose of the rest of the paper is to investigate the effect of different intentional mistuning patterns composed of sectors A and B, and to try to find the pattern which optimizes both the 1F and 1T modes simultaneously.

4. GLOBAL OPTIMIZATION OF THE MISTUNED STRUCTURE

When the system is mistuned, the solution methodology employed in Section 3 can no longer be applied. To determine the exact motion of such structures, the equation of motion of the full system must be solved. In practise, this procedure is not used because it requires large memory space to store the mass, damping, and stiffness matrices, and the computation time would be excessively long, mainly due to the computation of the nonlinear forces for all sectors. In this paper, we employ a recent nonlinear ROM methodology called the Substructuring method based on Nonlinear Cyclic Reduction (SNCR) [24] to compute the frequency forced responses of systems with different intentional mistuning patterns. This approach is briefly explained in Section 4.1, and then tested and analyzed for cyclic symmetric structures in Section 4.2. In Section 4.3, it is applied to solve the optimization problem on a mistuned structure.

4.1 Short description of the ROM methodology

The SNCR [24] employs a substructuring approach [32] in which the full structure is broken down into N substructures (the N sectors). Hence, for each different kind of sector (two in this case), the associated cyclic nonlinear normal modes (CNNMs) must be computed. The full reduced structure is obtained by assembling the reduced sectors on their boundary control coordinates. To ensure a compact system, we employ the strategy proposed in Section 4.2 of [24] and only compute the CNNMs

for the 0, 2, 6 and 10−th nodal diameters, for both the 1F and 1T modes. Once the reduced model is obtained, a frequency force response synthesis can be simulated. To ensure fast computation, the SNCR substitutes the nonlinear forces by the CNNMs.

4.2 Performance and validation of the method

The reduced basis is made up of $2 \times 4 = 8$ CNNMs (two kinds of sector: A and B, and four nodal diameters) for the 1F and 1T modes. These modes are evaluated only once and can be used to simulate the frequency forced response of any intentional mistuning pattern (any combination of sectors A and B) excited around either the 1F or 1T frequency. The purpose of the following study is to show the accuracy and performance of the SNCR when applied to the current FEM. Since the reference method, presented in Section 3.1, only handles cyclic symmetric structures, four such structures were considered as test cases: the $(A)_{24}$, $(B)_{24}$, $(AB)_{12}$, and $(ABBA)_6$ structures. The notation $(X)_Y$ denotes the full 24-sector system composed of a supersector X which is repeated Y times. For these four systems, and thus in total eight cases (four systems and two modes), the SNCR was applied and compared with the methodology explained in Section 3.1 which acts as the reference method. Note that for the reference method, supersectors (composed of standard single sectors put next to each other) must be used for the AB and ABBA cases, whereas the SNCR employs a reduction basis composed of the CNNMs of sectors A and B taken independently, whatever the test case.

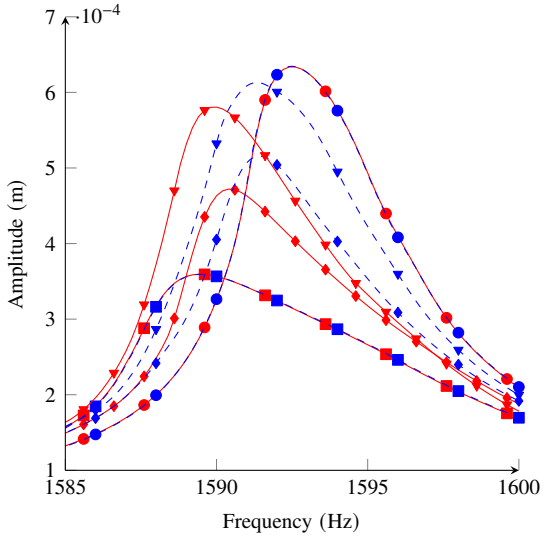

FIGURE 5: FREQUENCY FORCED RESPONSES FOR THE 1F MODE. (—): REFERENCE METHOD; (- -): SNCR. THE MARKERS (■), (●), (♦), AND (▼) DENOTE THE $(A)_{24}$, $(B)_{24}$, $(AB)_{12}$, AND $(ABBA)_6$ STRUCTURES.

Figure 5 represents the maximal displacement of the four test cases around the 1F natural frequency for the reference method and the SNCR. For the $(A)_{24}$ and $(B)_{24}$ systems, the results match perfectly. For the $(AB)_{12}$, and $(ABBA)_6$ structures, discrepancies can be observed: a shift of approximately 1 Hz in the resonant frequency peaks, and an error in the maximal amplitude of approximately 8% for the $(AB)_{12}$ case and 5% for the $(ABBA)_6$ case.

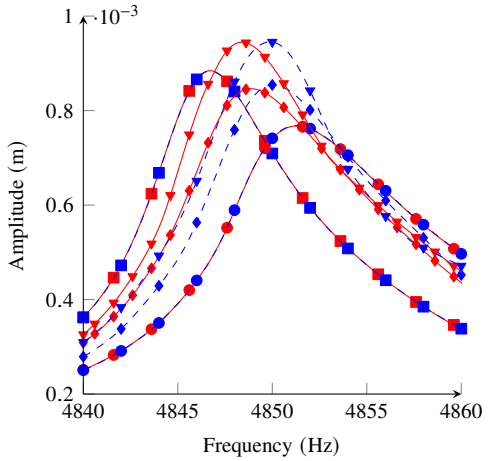

FIGURE 6: FREQUENCY FORCED RESPONSES FOR THE 1T MODE. (—): REFERENCE METHOD; (- -): SNCR. THE MARKERS (■), (●), (♦), AND (▼) DENOTE THE $(A)_{24}$, $(B)_{24}$, $(AB)_{12}$, AND $(ABBA)_6$ STRUCTURES.

Figure 6 represents the maximal displacement around the 1T frequency. For all four cases, the SNCR results provide a good match with the reference. Small discrepancies can be observed for the $(AB)_{12}$ and $(ABBA)_6$ structures (the amplitude error is below 2%) but the results are much more satisfactory overall than those obtained for the 1F mode.

In order to explain these different results, we can focus on the deformed shapes induced by the different values of μ. Figure 5 shows that, for the 1F mode, the difference in maximal amplitude between the $(A)_{24}$ and $(B)_{24}$ structures is 43% which is necessarily associated with significant different deformed shapes. However, for the 1T mode, the level of vibration of the $(B)_{24}$ structure is only 14% lower than the $(A)_{24}$ structure. The deformed shapes of sectors A and B are thus closer in this case.

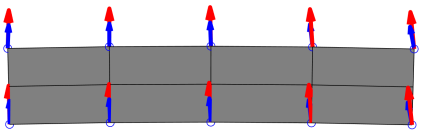

FIGURE 7: ILLUSTRATION OF THE DEFORMED SHAPE OF THE RIGHT UDP BOUNDARY SURFACE FOR THE 1F MODE. DIRECTION AND AMPLITUDE OF THE MAXIMAL DISPLACEMENT FOR: [→] THE $(A)_{24}$ STRUCTURE, AND [→] THE $(B)_{24}$ STRUCTURE.

Because the only difference between the designs of sectors A and B is their μ-value, the deformed shapes may be particularly different around the contact area. The contact area is close to the cyclic boundary DOFs which get assembled in the SNCR. Although the displacement is imposed continuously at the boundary, these different deformed shapes may create discrepancies in the assembling step when sectors A and B are put together. Figure 7 illustrates the deformed shape of the boundary surface of the right UPD (see Figure 1b) for the $(A)_{24}$ and $(B)_{24}$ structures

at their respective maximum resonant peak. On the left side of the boundary surface, the direction of motion is approximately the same, but its amplitude is greater for the $(B)_{24}$ structure. On the right side of the boundary surface, the direction and amplitude do not match. The difference in deformed shape can also be confirmed by Figures 5 and 6. First, the level of error between the reference and SNCR methods is higher overall for the 1F than for the 1T mode. This is because the deformed shapes between sectors A and B are similar in the 1T mode but significantly different in 1F. Furthermore, the $(AB)_{12}$ structure gives the largest error for both modes as sectors A and B keep alternating.

Despite these differences, the SNCR provides the correct trends in all cases. For example, for the 1F mode, the optimal case is the $(A)_{24}$ structure, followed in order by the $(AB)_{12}$, the $(ABBA)_6$ and then the $(B)_{24}$ structures. Moreover, the computation time of the SNCR is generally lower that of the reference, as highlighted in Table 1. The computation of a single CNNM lasts around 3 h but is performed only once. When the size of the supersector increases (from a single sector A to AB, and then to ABBA), the reference method gets more unknowns, whereas the SNCR keeps a constant number of generalized control coordinates. One of the main benefits of the SNCR is that it can be used for any intentional mistuning pattern, whereas the reference method is limited to cyclic structures with a small supersector size.

Modes	Systems	**No. of unknowns**		**Comp. time (in** h)	
		SNCR	Reference	SNCR	Reference
1F	$(A)_{24}$	672	1530	1.2	1.2
	$(B)_{24}$	672	1530	1.6	1.2
	$(AB)_{12}$	672	3060	1.4	5.7
	$(ABBA)_6$	672	7120	1.6	32.5
1T	$(A)_{24}$	672	1530	2.1	1.5
	$(B)_{24}$	672	1530	1.5	1.5
	$(AB)_{12}$	672	3060	1.9	6.3
	$(ABBA)_6$	672	7120	1.7	35.8

TABLE 1: PERFORMANCE OF THE SNCR. THE SIMULATIONS WERE RUN ON A INTEL(R) CORE(TM) I7-7700 @ 3.6 GHZ COMPUTER.

In light of the accuracy and efficiency of the SNCR, a series of simulations for multiple intentional mistuning patterns were performed next. The purpose was to establish the optimal pattern which minimizes the maximal displacement for both the 1T and the 1F modes. Although the SNCR does not provide exact results on this model, it does at least simulate the correct trends. Note that without such a method, the computation of an arbitrary intentional mistuning pattern would require the equation of motion of the full structure to be solved, which is not feasible in a reasonable amount of time.

4.3 Finding the optimal mistuning pattern for both the 1F and 1T modes

Sector A was chosen to optimize the 1F mode, and sector B the 1T mode. The purpose of this section is to find the optimal A-B pattern that can minimize the displacement of both modes simultaneously. There are different possibilities to perform such a task. The most obvious would be to compute the frequency forced responses for all possible combinations ($\approx 2^N/N$) [33]. This would require the computation of too many nonlinear simulations, however, and is not currently feasible. In [34], Choi et al. proposed to use a genetic algorithm to optimize an intentional mistuning pattern for a linear problem. Such a procedure could be considered in this paper, but the main downside of the genetic algorithm is that we cannot ensure the global convergence of the solution. In [33], the authors used a subspace optimization strategy. Based on [34, 35], it was shown, in a linear system, that for weakly coupled blades, the optimized pattern exhibited frequent switches between the A and B sectors. However, for strong coupling, the optimized pattern did not present many switches. Such a strategy is commonly used, as in [36], and will be employed next.

Two optimized patterns were studied. The first was composed of AB or BA supersectors to account for weakly coupled blades; the second pattern was composed of AA or BB supersectors and accounts for strong coupling. For each optimization problem and each mode, there were 352 ($\approx 2^{12}/12$) simulations to perform (and not $\approx 2^{24}/24$ because a supersector composed of two standard sectors was considered here). The task was still significant as a total of $2 \times 2 \times 352 = 1408$ nonlinear simulations must be carried out. Parallel computations were employed to perform this in a reasonable amount of time.

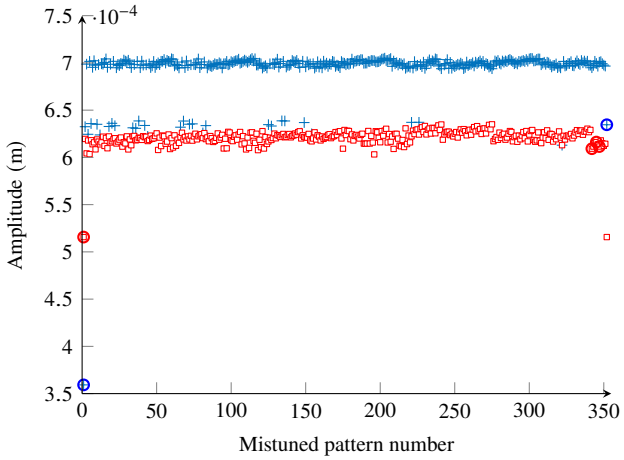

FIGURE 8: MAXIMAL AMPLITUDE DISPLACEMENT FOR THE DIFFERENT MISTUNING PATTERNS FOR THE 1F MODE. (□): COMBINATION OF AB AND BA; (+): COMBINATION OF AA AND BB.

Figure 8 (respectively Figure 9) represents the maximal displacement with respect to the mistuning pattern number for the 1F mode (respectively 1T mode). The red squares correspond to the structures composed of AB and BA supersectors, and the blue crosses are those containing AA and BB supersectors. For both modes, the AB/BA structures show smaller displacements than the AA/BB ones. Based on [33], this would mean that the blades are weakly coupled in the current model. The blades are coupled by the disk and the dampers. However, for the latter, vibratory energy is lost due to friction and may explain the weak coupling

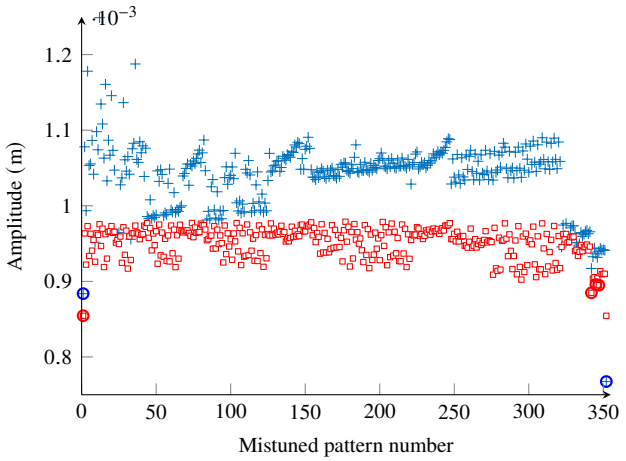

FIGURE 9: MAXIMAL AMPLITUDE DISPLACEMENT FOR THE DIFFERENT MISTUNING PATTERNS FOR THE 1T MODE. (□): COMBINATION OF AB AND BA; (+): COMBINATION OF AA AND BB.

observed.

Using the maximal displacement of the 1F and 1T modes (noted $|\max u_{1F}|$ and $|\max u_{1T}|$), the best intentional mistuned pattern can be determined. Two different objective functions that must be minimized are considered:

$$\text{crit}_{\text{sum}} = |\max u_{1F}| + |\max u_{1T}|\,, \tag{7}$$

and

$$\text{crit}_{\text{fatigue}} = |\max u_{1F}| + \frac{\omega_{1T}}{\omega_{1F}} |\max u_{1T}|\,. \tag{8}$$

The first function, crit_{sum}, is simply the sum of the amplitudes. The second takes into account the frequencies of each mode and can be related to the fatigue of the system. Tables 2 and 3 provide the first six best intentional mistuning patterns for the two criteria. The rank, value of the objective functions and corresponding mistuning pattern are provided. The mistuned pattern numbers are also given in Tables 2 and 3 to help identify the best structures in Figures 8 and 9 (see the larger markers). The same six mistuned patterns are obtained in both cases. Out of these six, three have been studied in Section 3.2 the $(\text{A})_{24}$, $(\text{B})_{24}$, and $(\text{AB})_{12}$ structures. The fourth, fifth and sixth best patterns are respectively $(\text{2A2B1A1B})_4$, $(\text{2A2B1A1B1A1B})_3$ and 2A2B1A1B2A2B1A1B1A1B1A1B2A2B1A1B1A1B (noted MP345 in Tables 2 and 3). In real bladed disk designs, the $(\text{A})_{24}$ and $(\text{B})_{24}$ structures are not suited due to flutter phenomena [15, 37, 38]. Moreoever in the presence of random mistuning (which is unavoidable in reality), the structures showing a pattern that repeats itself are subjected to a large amplification factor due to the frequency splitting of the degenerated nodal diameter (such as the tenth nodal diameter under study). As a consequence, the mistuned pattern noted MP345 may be the best compromise here.

A more complete study would consist of evaluating the amplification factor of these six mistuned patterns with respect to random mistuning deviation. Such an analysis is beyond the scope of this work. Instead, in the next Section we propose a sensitivity analysis of the influence of random mistuning on the maximal displacement of the structure.

Rank	Mistuning pattern	Pattern number	Function value
1	$(\text{A})_{24}$	1 for AA/BB	1.2×10^{-3}
2	$(\text{AB})_{12}$	1 for AB/BA	1.4×10^{-3}
3	$(\text{B})_{24}$	352 for AA/BB	1.4×10^{-3}
4	$(\text{2A2B1A1B})_4$	342 for AB/BA	1.5×10^{-3}
5	$(\text{2A2B1A1B1A1B})_3$	347 for AB/BA	1.5×10^{-3}
6	MP345	345 for AB/BA	1.5×10^{-3}

TABLE 2: OPTIMAL MISTUNING PATTERNS FOR THE FUNCTION crit_{sum}.

Rank	Mistuning pattern	Pattern number	Function value
1	$(\text{B})_{24}$	352 for AA/BB	3.0×10^{-3}
2	$(\text{A})_{24}$	1 for AA/BB	3.0×10^{-3}
3	$(\text{AB})_{12}$	1 for AB/BA	3.1×10^{-3}
4	$(\text{2A2B1A1B})_4$	342 for AB/BA	3.3×10^{-3}
5	$(\text{2A2B1A1B1A1B})_3$	347 for AB/BA	3.3×10^{-3}
6	MP345	345 for AB/BA	3.3×10^{-3}

TABLE 3: OPTIMAL MISTUNING PATTERNS FOR THE FUNCTION $\text{crit}_{\text{fatigue}}$.

4.4 Sensitivity of the systems to random mistuning

As explained in [24], the SNCR can handle random mistuning. In this work, the influence of random mistuning on the $(\text{A})_{24}$, $(\text{AB})_{12}$, $(\text{2A2B1A1B})_4$ and MP345 structures was investigated. The mistuning was modeled by modifying the internal modes in the Craig-Bampton reduction following a normal distribution with a standard deviation equal to 10% (as proposed in [16]). The sensitivity of the $(\text{A})_{24}$, $(\text{AB})_{12}$, $(\text{2A2B1A1B})_4$ and MP345 structures to a random mistuning with deviation equal to 10% was investigated. Only a single simulation was performed on the 1F mode and the associated results are presented in Figure 10.

As expected, for each system (denoted by different markers in Figure 10), the presence of random mistuning leads to a higher maximal displacement response. The amplification response factor (defined as the ratio between the maximal displacement of the randomly mistuned structure and the maximal displacement of the initial structure) was computed for each system. Their values are equal to 14%, 17%, 8% and 6% for the $(\text{A})_{24}$, $(\text{AB})_{12}$, $(\text{2A2B1A1B})_4$ and MP345 systems respectively. Although the $(\text{A})_{24}$, $(\text{AB})_{12}$ show better results in Tables 2 and 3 than the MP345 system, they are much more sensitive to random mistuning and as a consequence should not be kept as optimal candidates. On the other hand, the MP345 system (which does not contain any supersector repetition) is the least sensitive to random mistuning and may be considered the optimal solution.

CONCLUSION

This paper proposes an original application for an intentional mistuning nonlinear finite-element structure. Two kinds of sector were defined with different friction coefficients on the contact

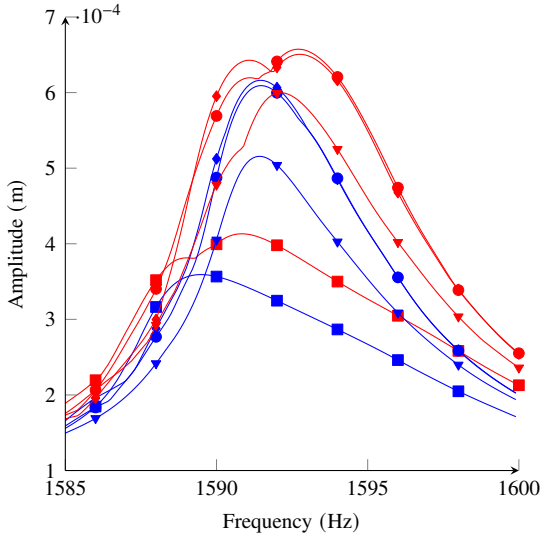

FIGURE 10: FREQUENCY FORCED RESPONSES FOR THE 1F MODE FOR THE SIX BEST STRUCTURES. (—): WITHOUT RANDOM MISTUNING; (—): WITH RANDOM MISTUNING. THE MARKERS (■), (▼), (●), AND (♦) DENOTE THE $(A)_{24}$, $(AB)_{12}$, $(2A2B1A1B)_4$ AND MP345 SYSTEMS.

area between the blades and the UPDs. The first kind of sector (A) was chosen to optimize the maximal displacement of the associated tuned structure for the first flexural mode, whereas the second (B) optimizes the first torsional mode. An optimization procedure was then performed to determine the best intentional mistuned patterns. Patterns composed of alternating A and B sectors showed better characteristics than those composed of repeating A and/or B sectors because they simultaneously optimize the forced response around both the 1F and the 1T frequencies. This result is mode-dependent, and the optimal pattern may be different when focusing on modes in a veering zone. To the authors' knowledge, such optimization has never been proposed in the literature due to the complex nature of the system (mistuned and nonlinear). Through a subspace optimization strategy, the best six mistuned patterns were identified. In reality, some of the patterns are ill-suited due to aerodynamical considerations (such as flutter phenomena), as well as to the negative impact of random mistuning on the level of vibration of the structure. With these further constraints, a final optimal mistuned pattern was identified. It is interesting to note that it does not present any supersector repetition.

Perspectives of this work could consist in extensive studies on the random mistuning effect (for instance by performing a Monte-Carlo simulation). In light of the numerical results presented here, experimental tests could also be considered, such as the one presented in [39], to complete the study.

ACKNOWLEDGEMENT

The authors are grateful for the financial support of Safran Helicopter Engines.

REFERENCES

[1] Gola, Muzio M. and Gastaldi, Chiara. "Understanding Complexities in Underplatform Damper Mechanics." 2014. American Society of Mechanical Engineers Digital Collection. DOI 10.1115/GT2014-25240.

[2] Firrone, Christian, Zucca, Stefano and Gola, Muzio. "The effect of underplatform dampers on the forced response of bladed disks by a coupled static/dynamic harmonic balance method." *International Journal of Non-Linear Mechanics* Vol. 46 (2011): pp. 363–375. DOI 10.1016/j.ijnonlinmec.2010.10.001.

[3] Petrov, E. P. and Ewins, D. J. "Advanced Modeling of Underplatform Friction Dampers for Analysis of Bladed Disk Vibration." *Journal of Turbomachinery* Vol. 129 No. 1 (2007): pp. 143–150. DOI 10.1115/1.2372775.

[4] Pesaresi, L., Salles, L., Jones, A., Green, J. S. and Schwingshackl, C. W. "Modelling the nonlinear behaviour of an underplatform damper test rig for turbine applications." *Mechanical Systems and Signal Processing* Vol. 85 (2017): pp. 662–679. DOI 10.1016/j.ymssp.2016.09.007.

[5] Pesaresi, L., Armand, J., Schwingshackl, C. W., Salles, L. and Wong, C. "An advanced underplatform damper modelling approach based on a microslip contact model." *Journal of Sound and Vibration* Vol. 436 (2018): pp. 327–340. DOI 10.1016/j.jsv.2018.08.014.

[6] Gastaldi, Chiara and Gola, Muzio M. "Platform Centered Reduction: a Process Capturing the Essentials for Blade-Damper Coupled Optimization." *Journal of Engineering for Gas Turbines and Power* DOI 10.1115/1.4049187.

[7] He, Bingbing, Ouyang, Huajiang, Ren, Xingmin and He, Shangwen. "Dynamic Response of a Simplified Turbine Blade Model with Under-Platform Dry Friction Dampers Considering Normal Load Variation." *Applied Sciences* Vol. 7 No. 3 (2017): p. 228. DOI 10.3390/app7030228.

[8] Schwingshackl, C. W., Petrov, E. P. and Ewins, D. J. "Effects of Contact Interface Parameters on Vibration of Turbine Bladed Disks With Underplatform Dampers." *Journal of Engineering for Gas Turbines and Power* Vol. 134 No. 3 (2012). DOI 10.1115/1.4004721. Publisher: American Society of Mechanical Engineers Digital Collection.

[9] Panning, Lars, Sextro, Walter and Popp, Karl. "Spatial dynamics of tuned and mistuned bladed disks with cylindrical and wedge-shaped friction dampers." (2003). DOI https://doi.org/10.1155/S1023621X03000198. ISSN: 1023-621X Issue: 3 Pages: 219-228 Publisher: Hindawi Volume: 9.

[10] MacNeal, R. H. "NASTRAN cyclic symmetry capability. [application to solid rocket propellant grains and space antennas]." 1973.

[11] Thomas, D. L. "Dynamics of rotationally periodic structures." *International Journal for Numerical Methods in Engineering* Vol. 14 No. 1 (1979): pp. 81–102. DOI 10.1002/nme.1620140107.

[12] Mitra, Mainak and Epureanu, Bogdan I. "Dynamic modeling and projection-based reduction methods for bladed disks with nonlinear frictional and intermittent contact interfaces." *Applied Mechanics Reviews* Vol. 71 No. 5 (2019).

DOI 10.1115/1.4043083. Publisher: American Society of Mechanical Engineers Digital Collection.

[13] Petrov, E. P. "A method for use of cyclic symmetry properties in analysis of nonlinear multiharmonic vibrations of bladed disks." *Journal of Turbomachinery* Vol. 126 No. 1 (2004): p. 175. DOI 10.1115/1.1644558.

[14] Quaegebeur, Samuel, Chouvion, Benjamin and Thouverez, Fabrice. "Model reduction of nonlinear cyclic structures based on their cyclic symmetric properties." *Mechanical Systems and Signal Processing* Vol. 145 (2020): p. 106970. DOI 10.1016/j.ymssp.2020.106970.

[15] Castanier, Matthew P. and Pierre, Christophe. "Modeling and analysis of mistuned bladed disk vibration : Status and emerging directions." 2006. DOI 10.2514/1.16345.

[16] Lim, Sang-Ho, Bladh, Ronnie, Castanier, Matthew P. and Pierre, Christophe. "Compact, generalized component mode mistuning representation for modeling bladed disk vibration." *AIAA Journal* Vol. 45 No. 9 (2007): pp. 2285–2298. DOI 10.2514/1.13172.

[17] Vargiu, P., Firrone, C. M., Zucca, S. and Gola, M. M. "A reduced order model based on sector mistuning for the dynamic analysis of mistuned bladed disks." *International Journal of Mechanical Sciences* Vol. 53 No. 8 (2011): pp. 639–646. DOI 10.1016/j.ijmecsci.2011.05.010.

[18] Madden, Andrew, Epureanu, Bogdan I. and Filippi, Sergio. "Reduced-order modeling approach for blisks with large mass, stiffness, and geometric mistuning." *AIAA Journal* Vol. 50 No. 2 (2012): pp. 366–374. DOI 10.2514/1.J051140.

[19] Schwerdt L, Wallaschek J, Panning-von Scheidt L. "A model reduction method for blade disks with large geometric mistuning using partial reduced intermediate system model." (2020)Conference proceedings in Turboexpo 2020. To be published in ASME.

[20] Tang, Weihan, Baek, Seunghun and Epureanu, Bogdan I. "Reduced-order models for blisks with small and large mistuning and friction dampers." *Journal of Engineering for Gas Turbines and Power* Vol. 139 No. 1 (2017). DOI 10.1115/1.4034212.

[21] Pourkiaee, S. M. and Zucca, Stefano. "A reduced order model for nonlinear dynamics of mistuned bladed disks with shroud friction contacts." *Journal of Engineering for Gas Turbines and Power* Vol. 141 No. 1 (2019). DOI 10.1115/1.4041653. Publisher: American Society of Mechanical Engineers Digital Collection.

[22] Mashayekhi, F., Nobari, A. S. and Zucca, S. "Hybrid reduction of mistuned bladed disks for nonlinear forced response analysis with dry friction." *International Journal of Non-Linear Mechanics* Vol. 116 (2019): pp. 73–84. DOI 10.1016/j.ijnonlinmec.2019.06.001.

[23] Joannin, Colas, Chouvion, Benjamin, Thouverez, Fabrice, Ousty, Jean-Philippe and Mbaye, Moustapha. "A nonlinear component mode synthesis method for the computation of steady-state vibrations in non-conservative systems." *Mechanical Systems and Signal Processing* Vol. 83 (2017): pp. 75–92. DOI 10.1016/j.ymssp.2016.05.044.

[24] Quaegebeur, Samuel, Chouvion, Benjamin and Thouverez, Fabrice. "Nonlinear cyclic reduction for the analysis of mistuned cyclic systems." *Journal of Sound and Vibration* Vol. 499 (2021): p. 116002. DOI 10.1016/j.jsv.2021.116002.

[25] Tang, Weihan and Epureanu, Bogdan I. "Geometric optimization of dry friction ring dampers." *International Journal of Non-Linear Mechanics* Vol. 109 (2019): pp. 40–49. DOI 10.1016/j.ijnonlinmec.2018.11.001.

[26] Craig, Roy R. and Bampton, Mervyn C. C. "Coupling of substructures for dynamic analyses." *AIAA Journal* Vol. 6 No. 7 (1968): pp. 1313–1319. DOI 10.2514/3.4741.

[27] Krack, Malte, Tatzko, Sebastian, Panning-von Scheidt, Lars and Wallaschek, Jörg. "Reliability optimization of friction-damped systems using nonlinear modes." *Journal of Sound and Vibration* Vol. 333 No. 13 (2014): pp. 2699–2712. DOI 10.1016/j.jsv.2014.02.008.

[28] Krack, Malte, Salles, Loic and Thouverez, Fabrice. "Vibration Prediction of Bladed Disks Coupled by Friction Joints." *Archives of Computational Methods in Engineering* Vol. 24 No. 3 (2017): pp. 589–636. DOI 10.1007/s11831-016-9183-2.

[29] Nacivet, Samuel, Pierre, Christophe, Thouverez, Fabrice and Jézéquel, Louis. "A dynamic Lagrangian frequency–time method for the vibration of dry-friction-damped systems." *Journal of Sound and Vibration* Vol. 265 No. 1 (2003): pp. 201–219. DOI 10.1016/S0022-460X(02)01447-5.

[30] Poudou, Olivier and Pierre, Christophe. "Hybrid frequency-time domain methods for the analysis of complex structural systems with dry friction damping." *44th AIAA/ASME/ASCE/AHS/ASC Structures, Structural Dynamics, and Materials Conference*. American Institute of Aeronautics and Astronautics. DOI 10.2514/6.2003-1411.

[31] Cameron, T. M. and Griffin, J. H. "An alternating frequency/time domain method for calculating the steady-state response of nonlinear dynamic systems." *Journal of Applied Mechanics* Vol. 56 No. 1 (1989): pp. 149–154. DOI 10.1115/1.3176036.

[32] Tran, Duc-Minh. "Component mode synthesis methods using partial interface modes: Application to tuned and mistuned structures with cyclic symmetry." *Computers & Structures* Vol. 87 No. 17 (2009): pp. 1141–1153. DOI 10.1016/j.compstruc.2009.04.009.

[33] Han, Yun, Murthy, Raghavendra, Mignolet, Marc P. and Lentz, Jeff. "Optimization of intentional mistuning patterns for the mitigation of the effects of random mistuning." *Journal of Engineering for Gas Turbines and Power* Vol. 136 No. 6 (2014). DOI 10.1115/1.4026141. Publisher: American Society of Mechanical Engineers Digital Collection.

[34] Choi, B.-K., Lentz, J., Rivas-Guerra, A. J. and Mignolet, M. P. "Optimization of intentional mistuning patterns for the reduction of the forced response effects of unintentional mistuning: formulation and assessment." *Journal of Engineering for Gas Turbines and Power* Vol. 125 No. 1 (2003): pp. 131–140. DOI 10.1115/1.1498270.

[35] Rivas-Guerra, A. J. and Mignolet, M. P. "Local/global effects of mistuning on the forced response of bladed disks."

Journal of Engineering for Gas Turbines and Power Vol. 126 No. 1 (2004): pp. 131–141. DOI 10.1115/1.1581898. Publisher: American Society of Mechanical Engineers Digital Collection.

[36] Mbaye, Moustapha. "Conception robuste en vibration et aéroélasticité des roues aubagées de turbomachines." These de doctorat, Paris Est. 2009.

[37] Martel, Carlos, Corral, Roque and Llorens, José Miguel. "Stability Increase of Aerodynamically Unstable Rotors Using Intentional Mistuning." *Journal of Turbomachinery* Vol. 130 No. 1 (2008). DOI 10.1115/1.2720503.

[38] Biagiotti, Sara, Pinelli, Lorenzo, Poli, Francesco, Vanti, Federico and Pacciani, Roberto. "Numerical Study of Flutter Stabilization in Low Pressure Turbine Rotor with Intentional Mistuning." *Energy Procedia* Vol. 148 (2018): pp. 98–105. DOI 10.1016/j.egypro.2018.08.035.

[39] Gastaldi, Chiara, Berruti, Teresa M., Gola, Muzio M. and Bessone, Andrea. "Experimental Investigation on Real Under-Platform Dampers: The Impact of Design and Manufacturing." 2019. American Society of Mechanical Engineers Digital Collection. DOI 10.1115/GT2019-90416.